Precipitation and Attenuation Estimates from a High Resolution Weather Radar Network (PATTERN) – Design of the Experiment

Katharina Lengfeld

Katharina Lengfeld[1], Marco Clemens[1], Nicole Feiertag[1], Felix Ament[1]
[1]*Meteorological Institute, University of Hamburg, Bundesstrasse 55, 20146 Hamburg, Germany, katharina.lengfeld@zmaw.de*

1. Introduction

Precipitation plays an important role in driving the energy and hydrological cycle of the atmospheric boundary layer. High resolution in situ and ground based remote sensing observations are needed to gain detailed insight in these processes for flood forecasting, urban hydrology, hydro-meteorological applications and management of risk and uncertainty. Rainfall products of conventional radar systems used in nationwide or larger networks are generally based on reflectivity measurements at S- or C-band wavelength. These radar systems cannot meet all present and future demands of resolution. For the different practical applications the requested spatial resolution is 0.1 km with a temporal resolution of 1 minute or below (Einfalt, 2003). Therefore, radar systems which are capable of producing reliable and accurate quantitative estimates of rainfall at high temporal and spatial resolution are required. Besides the higher resolution, radars operating at high frequencies benefit from lower costs because of smaller antenna size compared to long wave radars (Bringi et al., 1990).

In recent years novel, low-cost high resolution weather radar (HRWR) systems have been developed. These systems are able to scan precipitation with spatial resolution of 60 meters in range and temporal resolution of 30 seconds. HRWRs operate in the X-band frequency range. As many authors stated since the early weather radar meteorology, microwaves are affected by attenuation due to rain (e.g. Atlas and Banks, 1951; Gunn and East, 1954, Wexler and Atlas, 1963; Dutton, 1967; Atlas and Ulbrich, 1977). The project *Precipitation and Attenuation Estimates from a High Resolution Weather Radar Network* (PATTERN) intends to demonstrate that a HRWR network can overcome this apparent drawback. In regions covered by more than one radar, it is possible to derive both intrinsic reflectivity and specific attenuation. The relation between specific attenuation and precipitation rate varies less than the commonly used relation between reflectivity and precipitation rate. Specific attenuation as additionally observed quantity will likely improve the accuracy of rain rate estimates.

2. Radar System

Within PATTERN, the University of Hamburg and the Max-Planck-Institute for Meteorology have set up a network consisting of four HRWRs near Hamburg, Germany, in 2011. The four radar positions Hungriger Wolf Tower (HWT), Moordorf (MOD), Quarnstedt (QNS) and Bekmünde (BKM) and their coverage are shown in Fig. 1. An additional X-Band radar, marked in blue in Fig. 1, will be placed on the roof of the *Meteorological Institute* of the University of Hamburg in summer 2012. This radar is located South-East of the PATTERN network.

Each radar measures with a range resolution of 60 meters in 1° steps. The time resolution is 30 seconds. The radars are about 10 to 15 km apart and have a maximum range of 20 km. Therefore, a large area exists within the network that is covered by at least two radars at the border and by up to four radars in the centre. Micro rain radars (MRR) are placed next to each radar and within the overlapping area to validate the precipitation measurements of the radar network.

The low-cost short-range HRWRs used in this study are modified ship navigation radars. They bridge the gap between quantitative rain indicators and high-end long range systems. Technical details of the used radar systems are summarised in Table 1. The radar front end including scanning unit is based on a standard navigation radar (see Fig. 2a). The high level signal processing, the data management and the radar control is PC-based. The original fan beam antenna is replaced by a high gain pencil beam antenna. Low side lobes are achieved using an offset parabolic dish. The antenna and scanning drive is protected by a low loss radome with air conditioning. The scanning scheme is azimuthal only. Fixed elevation angles can be adjusted for optimum operation according to the site conditions. Three of the network radars are set up on a 10 meters high steel tower mounted on the roof of a container (Fig. 2b). The fourth radar (HWT) is mounted on an already existing steal tower at the airport *Hungriger Wolf*.

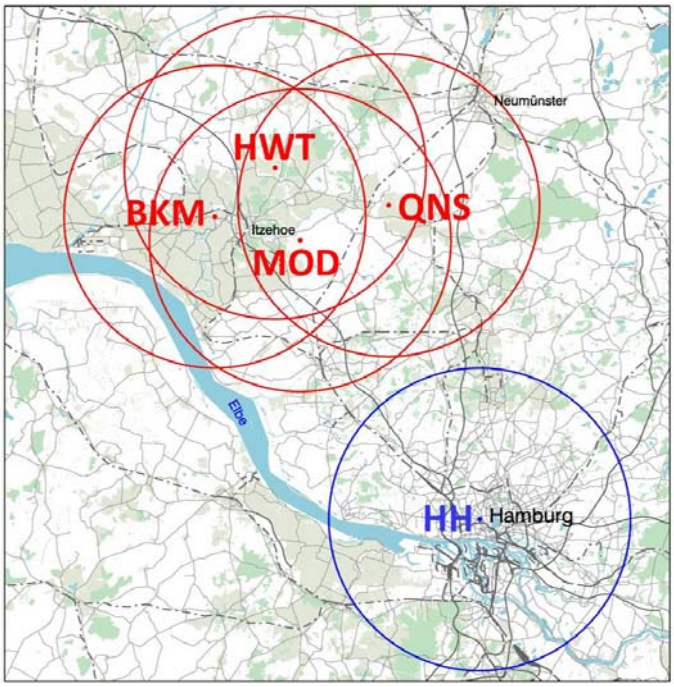

Fig. 1 *Positions of the four radars Hungriger Wolf Tower (HWT), Quarnstedt (QNS), Bekmünde (BKM) and Moordorf (MOD) marked as in red, the Hamburg radar (HH) marked in blue and their 20 km range.*

Table 1 *HRWR specifications*

Performance Parameters	**Specifications**
Range Resolution	60 m
Azimuth Resolution	2°
Time Resolution	30 s
Maximum Range	20 km
Calibration Accuracy	± 1dB
Transmit Power	25 kW
Frequency	9410 MHz
Pulse Width	0.08 µs
Pulse Repetition Rate	2100 Hz
Beam Width (6dB two way)	3°

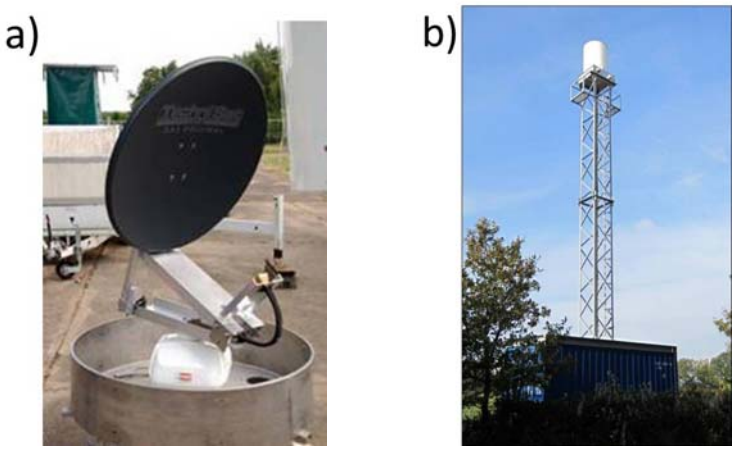

Fig. 2 *Modified ship radar with parabolic dish (a) and complete radar tower in Quarnstedt (b)*

3. Processing

Before the potential of the network can be exploited, erroneous data needs to be eliminated for single radar images. The radar image of raw data for January 23, 2012, 20:00:30 UTC in Moordorf is shown exemplary in Fig. 3a. The process chain containing the filters used to identify erroneous data points is depicted as a flowchart in Fig. 3b.

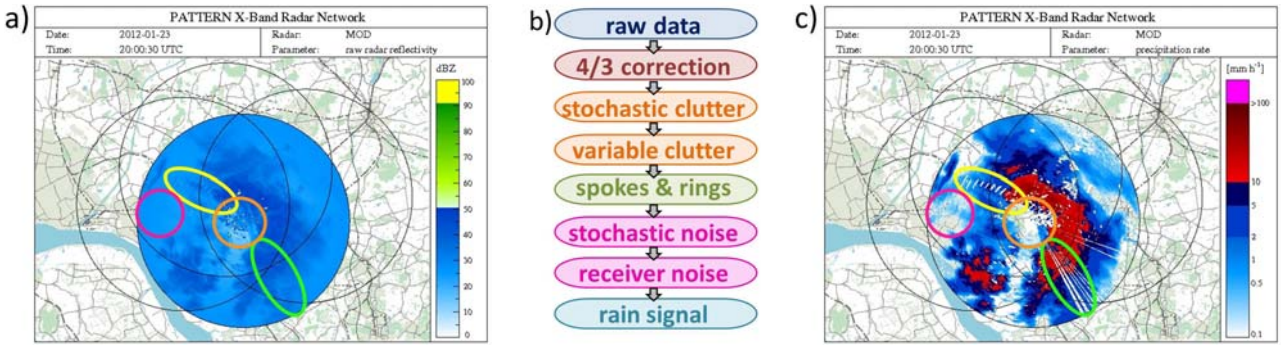

Fig. 3 *Raw data reflectivity field on January 23, 2012, 20:00:30 UTC for Moordorf (a), flowchart of the filters that are applied to the raw data (b) and the resulting precipitation field (c). The coloured circles mark different kinds of disturbances: Pink marks receiver noise, oranger clutter, yellow rings and green spokes.*

In the first step, a 4/3 correction is applied. The earth surface is curved but the radar beam is straight. Therefore, the radar beam needs to be projected on the earth surface using a factor of 4/3 of the earth radius (Doviak and Zrnic, 1992).

Radar images are highly disturbed by clutter (encircled in orange in Fig. 3a) resulting in high reflectivity signals. It can be divided into two different kinds of clutter. The first type is static clutter, caused by houses, trees or other unmovable obstacles. This clutter is present in almost every data set at the same location. Therefore, we generated a clutter map from a rain free data set for each radar by marking pixels as static clutter that show reflectivity values in more than 95%

of the cases. The second type is the variable clutter, caused by moving obstacles like wind mills. This clutter is distributed randomly over the image and is identified by comparing image pixels to their surrounding pixels. The texture of reflectivity is calculated as the mean of the squared reflectivity difference between two adjacent gates. Each gate consists of 31 pixels in radial direction. Another clutter indicator is the frequency of sign changes in the reflectivity gradient in a certain direction (we use radar radial direction). If the squared reflectivity difference (TDBZ) or the number of sign changes (SPIN) is higher than a certain threshold, the pixel is marked as clutter (Hubbert et al., 2009a, 2009b).

Other disturbances affect whole azimuth angles or certain distances from the radar. The so-called spokes are caused for example by the signal of other radars and mostly appear in the radar image as line segments of high reflectivity. In Fig. 3a the spokes encircled in green can hardly be seen because of the background noise. To identify these spokes the difference in reflectivity between one pixel and the neighbouring pixel in azimuth direction is calculated. The centre of a spoke is characterised by a sign change in the differences. Azimuth angles with more than a certain number of sign changes are marked as spokes. High reflectivity values can also be found as rings or parts of rings around the radar centre (marked in yellow in Fig. 3a). The identification procedure is similar to the spoke identification, except for calculating differences along radar beams instead of along azimuth angles.

To distinguish between stochastic noise and actual precipitation signal, the reflectivity within a 3 times 3 window around a pixel is considered. If 5 or more neighbouring pixels have positive reflectivity values the pixel is considered as precipitation, otherwise it is considered as stochastic noise. The receiver noise (e.g. within the pink circle) is eliminated with the help of a function that increases with the squared distance to the radar.

The reflectivity is finally converted to precipitation signal by using a common z-R relation. After applying all filters, we get precipitation fields for each radar. Fig. 3c illustrates the precipitation field for January 20, 2012, 20:00:30 UTC at the Moordorf radar. The background noise (e.g. encircled in pink), where no reflectivity from objects is measured is removed. The spokes in the green circle and the rings in the yellow circle are also eliminated. These phenomena overlay the actual precipitation signal. Therefore, by removing spokes or rings, precipitation signal can also be lost. The same is true for clutter. Most clutter is located in the centre close to the radar (orange circle). Precipitation that occurs close to the radar will be removed by the clutter filter.

4. First Results

The precipitation fields at all four radars for January 23, 2012, 20:00:30 UTC are shown in Fig. 4. The centre of the precipitation area with rain fall more than 10 mm/h is located in the middle of the radar covered area. Large data gaps are evident in Fig. 4 due to spokes, rings and clutter in all four radar images. For the HWT radar in the upper right panel of Fig. 4, the removal of clutter in the centre of the image is particularly evident, because the rain field is located right above

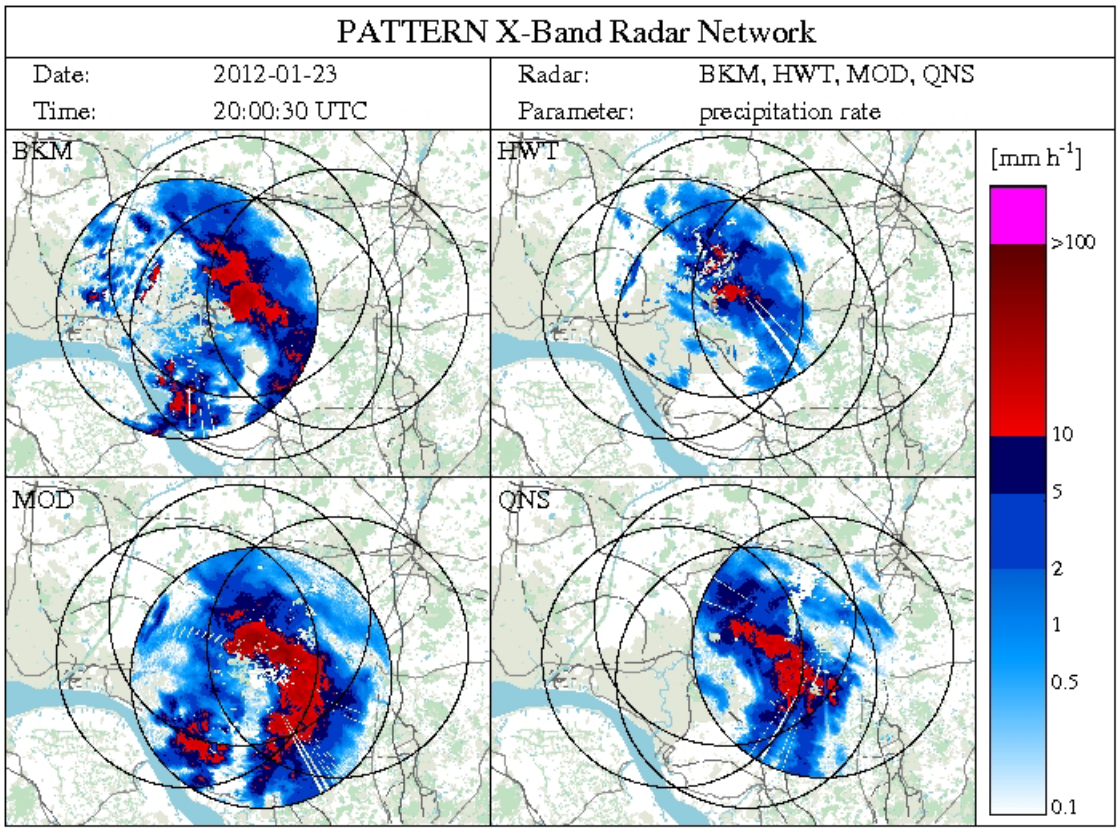

Fig. 4 *Precipitation rate at all four radars of the network on January 23, 2012, 20:00:30 UTC.*

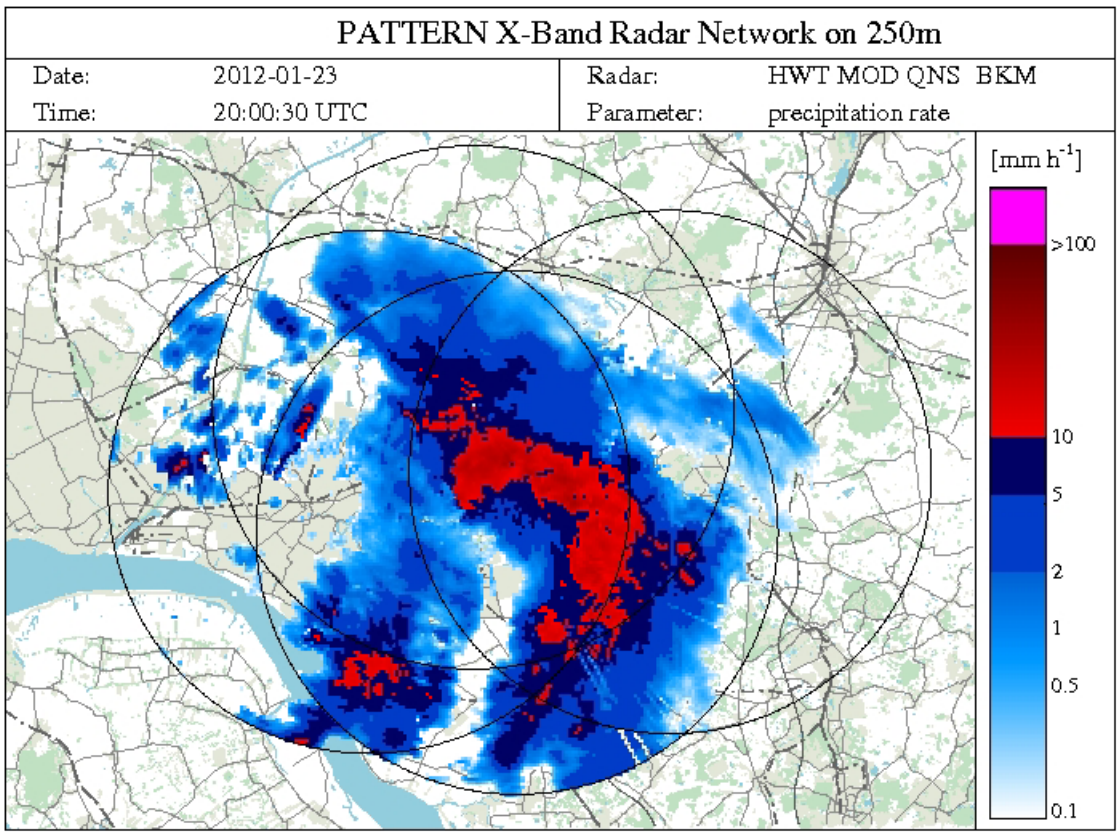

Fig. 5 *Composite of all four radars for precipitation rate on January 23, 2012, 20:00:30 UTC.*

the radar. The level of precipitation rate is clearly lower for HWT than for the other radars, probably due to attenuation. Some parts of the precipitation field, e.g. in the South of the HWT radar covered area, where the BKM and the MOD radar show precipitation, are removed by the background noise filter.

Having a network of radars is a big advantage. Most areas within the network are covered by more than one radar. Missing values of one radar can be replaced by measurements of one or more of the others. Therefore, a composite of all radars is calculated on a rotated Cartesian grid. I.e., the equator is shifted into our measurement site to allow for equidistant grid cells. We use a grid resolution of 250 m. The resolution of the radar is artificially enhanced by dividing each azimuth angle into 0.1° steps. Thus, we make sure that the grid boxes far away from the radar contain at least one radar pixel. Each radar pixel is assigned to the grid cell it is located in and the average of the reflectivity values of all radar pixels in a certain grid is calculated.

In Fig. 5 the precipitation rate is shown as composite of all four radars for January 23, 2012, 20:00:30 UTC. Most gaps in the data where spokes, rings or clutter occurred are covered by other radars. Therefore, no interpolation of the data within single radar images is necessary. Although precipitation levels are not the same yet for all radars, the composite shows smooth transitions from one radar to another. Some of the spokes are still apparent in Fig. 5 because of the different precipitation levels, but most spokes, rings and clutter gaps are removed by calculating the composite.

4. Outlook

The radar network is operational since autumn 2011. We intend to generate a unique multi-year data set of the HRWR network. This data set will be a helpful tool to develop and improve networked radar retrieval algorithms and gives us the opportunity to examine the accuracy of these retrievals in practise.

Radar measurements in the X-Band range are highly influenced by attenuation. Our HRWR network can overcome this apparent drawback. Currently a retrieval for two-dimensional rain fields in regions covered by more than one radar is developed. In a first step an idealized one-dimensional setup along connecting lines of two radar systems is computed. In this model based study the spatial distribution of intrinsic reflectivity and specific attenuation is known. A developed forward operator simulates the observed reflectivity. Backwards the retrieval is able to identify nearly exactly the intrinsic reflectivity. Three different methods for the backward operator are implemented. The first algorithm is based on Chandrasekar and Lim (2008), the second algorithm is based on a linear system of equation and the third algorithm uses the analytical solution of the intrinsic reflectivity. This most practical retrieval will be extended to the two-dimensional case.

To validate the potential of the radar network on local and regional scales 7 MMRs are placed within the measurement site. A MRR is located at every radar and three MRRs are located in the area covered by all four radars. Additional rain gauges and other radar products will be used for a comprehensive inter-comparison with our HRWR network.

Acknowledgment

The authors thank Hans Münster for preparing the ship navigation radars, for installing and maintaining the network and for all his technical support.

The project *Precipitations and Attenuation Estimates from a High Resolution Weather Radar Network* (PATTERN) is funded by the Deutsche Forschungsgesellschaft (DFG).

References

Atlas D., Banks H.C., 1951: The interpretation of Microwave Reflections from Rainfall. *J. Meteor*., **8**, 271-282

Atlas D., Ulbrich C.W., 1977: Path- and Area-Integrated Rainfall Measurements by Microwave Attenuation in the 1-3 cm Band. *J. Appl. Meteor*., **16**, 1322-1331

Bringi V.N., Chandrasekar V., Balakrishnan N., Zrnic D.S, 1990: An Examination of Propagation Effects in Rainfall on Radar Measurements at Microwave Frequencies. *J. Atmos. Oceanic Technol*., **7**, 829-840

Chandrasekar V., Lim S., 2008: Retrieval of Reflectivity in a Networked Radar Environment. *J. Atmos. Oceanic Technol.*, **25**, 1755-1767

Doviak R.J., Zrnic D.S., 1993: *Doppler Radar and Weather Observations*. 2nd Edition, Academic Press

Dutton E.J., 1967: Estimation of Radio Attenuation in Convective Rainfalls. *J. Appl. Meteor*., **6**, 622-668

Einfalt T., 2003: A user perspective in Germany: What is Expected by Agencies and Government from Radar Data? *Int. J. River Basin Management*, **1**, 1-5

Gunn K.L.S., East T., 1954: The Microwave Properties of Precipitation Particles. *Quart. J. R. Meteor. Soc*., **80**, 522-545

Hubbert J.C., Dixon M., Ellis S.M., Meymaris G., 2009a: Weather Radar Ground Clutter. Part I: Identification, Modelling, and Simulation. *J. Atmos. Oceanic Technol*., **26**, 1165-1180

Hubbert J.C., Dixon M., Ellis S.M., 2009b: Weather Radar Ground Clutter. Part II: Real-Time Identification and Filtering. *J. Atmos. Oceanic Technol.*, **26**, 1181-1197

Wexler R., Atlas D., 1963: Radar Reflectivity and Attenuation of Rain. *J. Appl. Meteor.*, **2**, 276-280